J Math Chem (2015) 53:718–736
DOI 10.1007/s10910-014-0453-7

ORIGINAL PAPER

Systematically altering the apparent topology of constrained quantum control landscapes

A. Donovan · H. Rabitz

Received: 20 November 2014 / Accepted: 3 December 2014 / Published online: 24 December 2014

Abstract A quantum control experiment typically seeks a shaped electromagnetic field to drive a system towards a specified observable objective. The large number of successful experiments can be understood through an exploration of the underlying quantum control landscape, which maps the objective as a function of the control variables. Specifically, under certain assumptions, the control landscape lacks suboptimal traps that could prevent identification of an optimal control. One of these assumptions is that there are no restrictions on the control variables, however, in practice control resources are inevitably constrained. The associated constrained quantum control landscape may be difficult to freely traverse due to the presence of limited resource induced traps. This work develops algorithms to (1) seek optimal controls under restricted resources, (2) explore the nature of apparent suboptimal landscape topology, and (3) favorably alter trap topology through systematic relaxation of the constraints. A set of mathematical tools are introduced to meet these needs by working directly with dynamic controls, rather than the prior studies that employed intermediate so-called kinematic control variables. The new tools are illustrated using few-level systems showing the capability of systematically relaxing constraints to convert an isolated trap into a level set or saddle feature on the landscape, thereby opening up the ability to find new solutions including those of higher fidelity. The results indicate the richness and complexity of the constrained quantum control landscape upon considering the tradeoff between resources and freedom to move on the landscape.

Keywords Quantum control · Quantum theory · Constrained quantum control · Constrained quantum control landscapes

A. Donovan · H. Rabitz (✉)
Department of Chemistry, Princeton University, Princeton, NJ 08544, USA
e-mail: hrabitz@princeton.edu

1 Introduction

Many quantum control experiments aim to identify a shaped electromagnetic field to enable reaching high fidelity of a desired observable as a result of tailored manipulation of the system's dynamics. Improvements in pulse-shaping, detection, and learning algorithms have led to a large number of successful quantum control experiments [1]. The search for a set of optimal control variables occurs on an underlying quantum control landscape [2], defined as the observable as a function of the control variables. Upon satisfaction of three assumptions, the control landscape has been found to be free of suboptimal traps [2]. If such traps were present they could hinder ready traversal of the landscape to achieve complete control. The aforementioned assumptions are that (1) the quantum system is controllable [3,4], (2) the set of time-dependent functions forming the matrix $\delta U(T,0)/\delta\varepsilon(t)$ is full rank, and (3) the control variables may be freely accessed without constraint. Here the control is $\varepsilon(t), 0 \leq t \leq T$, and the time evolution operator $U(t,0)$ is evaluated at the final time T where the control performance is evaluated. Assumption (3) is of prime interest for study as control resources for constructing $\varepsilon(t)$ are inevitably restricted in the laboratory. Thus the present work explores the impact on apparent landscape topology when assumption (3) is not fully satisfied. Here we refer to the evident new and possibly restrictive landscape features as *apparent*, since they arise on the nominally trap-free landscape due to constraints on the controls. In regard to these circumstances, numerical studies have considered quantum control scenarios with spectral component restrictions [5–7] and limitations on available phase controls [8,9]. An important research goal is to attain a general understanding of how constraints on control resources affect optimal performance. The present work develops mathematical techniques to explore the constrained quantum control landscape topology and alter the apparent landscape features by systematically relaxing the control constraints. The ability to alleviate constraint-induced landscape limitations (e.g., traps) opens up the prospect of considering the tradeoff between resources and control performance.

As a specific illustration of the concepts above, here we consider simulations with the goal of optimizing the state-to-state transition probability $P_{i\to f}$ at time T,

$$P_{i\to f} = |\langle f|U(T,0)|i\rangle|^2, \tag{1}$$

where $U(t,0)$ solves the time-dependent Schrödinger equation

$$\imath\hbar\frac{\partial}{\partial t}U(t,0) = H(t)U(t,0), \quad U(0,0) = \mathbb{1}. \tag{2}$$

The analysis and illustrations in this work are based on working with an N-level quantum system described by a reference Hamiltonian H_0 and a field coupling transition dipole μ so that

$$H(t) = H_0 - \mu\varepsilon(t). \tag{3}$$

This paper is concerned with the impact of a constrained control $\varepsilon(t)$ upon the apparent landscape topology, as well as the potential gains offered by systematic relaxation

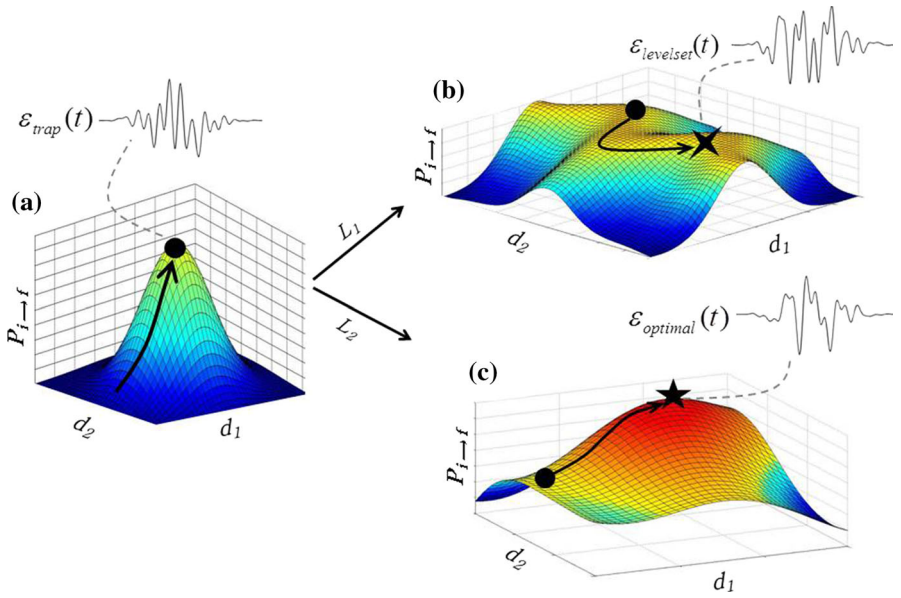

Fig. 1 (Color online) Schematic illustration of possible topologies at apparent suboptimal critical points on the constrained quantum control transition probability $P_{i\to f}$ landscape. Here, d_1 and d_2 refer to two control variables for graphical purposes, but in practice there will generally be many controls employed to create a field $\varepsilon(t)$. **a** An initial $P_{i\to f}$ landscape climb (represented by the *curved path*) stops at a suboptimal trap denoted by the *black dot*, with the corresponding control field $\varepsilon_{trap}(t)$. This trap is an isolated point, where any variation to the controls would result in a lower $P_{i\to f}$ value. **b** A trap (*black dot*) is shown on a manifold of suboptimal solutions having the same value for $P_{i\to f}$. A trajectory can be taken along this manifold represented by the curved arrow, where $\varepsilon_{levelset}(t)$ is one member of a set of homologous control fields forming the manifold. **c** This case shows that the critical point is a saddle (i.e., truncated along the d_1 axis for graphical reasons), where further ascension of the landscape is possible, as represented by the *curved path*. A control field producting optimal, or at least improved performance is denoted by $\varepsilon_{optimal}(t)$. The *arrows* L_1 and L_2 correspond to possible topological transformations, i.e., from a suboptimal isolated point to a level set and saddle, respectively. Such transformations are implemented by managed relaxation of the original control constraint, as described in Sect. 2.4

of the constraints. Importantly, this work extends recent studies that employed kinematic (time-independent) control variables as a means to simplify an initial analysis of the constrained landscape [10–12]. Here we sidestep the kinematic variables to directly operate with the field $\varepsilon(t)$. Figure 1 schematically illustrates the goals of the mathematical tools in the paper, where it is understood that the sketches represent three distinct types of *constrained* transition probability landscapes described below. The controls in Fig. 1 are applied electromagnetic fields, but like situations may be generalized to consider any type of control variables; in addition, the same control issues apply to other observables besides the state-to-state transition probability. In Fig. 1a the trajectory is a gradient-based landscape ascent that is subject to an imposed constraint. For graphical purposes only two control variables d_1 and d_2 are shown, but in practice many more variables are likely used to create a field $\varepsilon(t)$. With significant constraints present, it may not be possible to achieve full control and a resource-limited suboptimal critical point may be encountered, which is represented by the black dot

and corresponding control field $\varepsilon_{trap}(t)$ in Fig. 1a. Understanding the topology of a suboptimal critical point on the control landscape entails examining the associated second-order Hessian matrix evaluated under the constraint conditions. The topology at the black dot in Fig. 1a is that of an isolated trap, which would be reflected by a negative definite Hessian. Two alternate topological circumstances are shown in Fig. 1b, c. Figure 1b shows how a trap (black dot) may exist on a manifold of suboptimal solutions having the same $P_{i\to f}$ value; such a trap circumstance corresponds to a negative semidefinite Hessian. Even when trapped at a suboptimal yield, having the freedom to move on a level set may open up the prospect of finding a field with desirable secondary properties such as robustness to noise. A trajectory along the level set is represented by the curved path, and $\varepsilon_{levelset}(t)$ corresponds to one member of a homologous family of distinct control fields identified by moving in the null space of the Hessian. Figure 1c illustrates a critical point (black dot) located at a saddle, with an indefinite Hessian. In the latter case, the landscape can be further ascended, producing a better yield or even possibly an optimal solution as denoted by $\varepsilon_{optimal}(t)$. In Fig. 1, the arrows L_1 and L_2 represent topological transformations changing an isolated trap into a level set and saddle, respectively. The paper presents the mathematical methodology to enable finding such transformations through systematic relaxation of the constrained resources.

The remainder of the paper is structured as follows. Section 2 sets out a gradient-based technique to ascend the transition probability landscape while the control satisfies an imposed constraint. The myopic nature of the search algorithm permits landscape ascent until a critical point is encountered. The means to determine the constrained Hessian are then presented in order to assess the nature of the critical point and especially permit relaxed constraints to implement transformations L_1 and L_2 in Fig. 1. Importantly, the mathematical tools presented in Sect. 2 are general and may be applied as the circumstances dictate. Each case needs to be assessed on its own merits, but with knowledge that eventual full constraint relaxation will enable a trap-free ascent of the landscape (considering as well that assumptions (1) and (2) above are also satisfied). Section 3 presents simple illustrative examples of the relaxation processes from Sect. 2, and Sect. 4 provides concluding remarks.

2 Mathematical techniques

In the laboratory, electromagnetic control fields are often expressed in terms of spectral amplitudes and/or phases. The remainder of this work will utilize the length-M vector β to represent the available control variables $\beta_m, m = 1, \ldots, M$, regardless of their specific nature. The control landscape is defined as an observable (here, $P_{i\to f}$) as a function of the control variables. We consider a single imposed constraint function $C(\beta)$ such that $C(\beta) = C_0$ is maintained at the constant value C_0 throughout a landscape traversal by varying β. Naturally the *form* of the function $C(\beta)$ is important for specifying the particular constraint. The relaxation of the constraint can involve changing C_0 as well as the form of $C(\beta)$. The latter circumstance is considered by including an additional set of constraint form variables $c_l, l = 1, \ldots, L$ such that $C(\beta) \to C(c, \beta)$. The capability of systematically relaxing the form of C opens

up the prospect for the topological transformations set out in Fig. 1, which will be considered in Sect. 2.4.

2.1 Traversing the quantum control landscape with constrained controls

A constraint function C is incorporated into the optimization of $P_{i\to f}$, and the algorithm uses a variation of the D-MORPH technique [13]. The form of the constraint will be specified as needed (i.e., in Sect. 3). In addition, the present work considers a single constraint C on the control variables, and the formulation below may be readily generalized to the case of multiple constraints. For the initial landscape ascent, the constraint form parameters c are considered fixed at their initial values, such that only the control variables β are permitted to vary. We introduce the variable $s > 0$ to label an evolving control trajectory, denoted $\beta(s)$, along the ascent. The goal is to maximize $P_{i\to f}$ over β while satisfying $C(\beta(s)) \equiv C(s) = C_0$. Thus, we wish to concomitantly enforce the climbing condition

$$\frac{dP_{i\to f}}{ds} = \nabla_\beta P_{i\to f}^\top \frac{\partial\beta}{\partial s} \geq 0 \tag{4}$$

and maintain the constraint

$$\frac{dC}{ds} = \nabla_\beta C^\top \frac{\partial\beta}{\partial s} = 0, \tag{5}$$

where $\nabla_\beta P_{i\to f}$ is the length-M gradient vector containing elements $\partial P_{i\to f}/\partial\beta_m$, $m = 1,\ldots,M$ and $\top$ denotes vector transpose. Likewise, $\nabla_\beta C$ contains the elements $\partial C/\partial\beta_m$. Such compact matrix–vector notation will be used throughout this work. The gradient $\partial P_{i\to f}/\partial\beta_m$ may be evaluated as [14]

$$\frac{\partial P_{i\to f}}{\partial\beta_m} = \frac{2}{\hbar}\mathrm{Im}\left[\int_0^T \langle i|U^\dagger(T,0)|f\rangle\langle f|U(T,0)U^\dagger(t,0)\frac{\partial H(t)}{\partial\beta_m}U(t,0)|i\rangle dt\right]. \tag{6}$$

The goal is to simultaneously satisfy Eqs. (4) and (5) by specifying a differential equation for $\beta(s)$. In this regard, the vector $\partial\beta/\partial s$ can be conveniently written in terms of a projector matrix $\mathcal{P}_C$ acting on a function (vector) f that may be freely chosen,

$$\frac{\partial\beta}{\partial s} = \mathcal{P}_C f \tag{7}$$

where

$$\mathcal{P}_C = \mathbb{1} - \nabla_\beta C(\nabla_\beta C^\top \nabla_\beta C)^{-1}\nabla_\beta C^\top, \tag{8}$$

and $\mathcal{P}_C$ projects into the direction orthogonal to $\nabla_\beta C$ in the β-space, thereby assuring that $C(\beta(s)) = C_0$ is maintained. The term $(\nabla_\beta C^\top \nabla_\beta C)$ is a scalar, which is assumed to be nonzero. Upon substituting Eq. (8) and the particular choice $f = \nabla_\beta P_{i\to f}$ into Eq. (7), then $\partial\beta/\partial s$ will satisfy Eqs. (4) and (5). A trajectory $\beta(s)$ will stop when $dP_{i\to f}/ds = 0$. This can occur when either a global landscape extremum is reached

(e.g., $P_{i\to f} = 1.0$), or when a suboptimal critical point is encountered. Importantly, the latter circumstance will generally arise when $\nabla_\beta P_{i\to f} \neq 0$. As such, setting $dP_{i\to f}/ds = 0$ in Eq. (4) and utilizing Eq. (7) leads to the trap condition of

$$\mathcal{P}_C \nabla_\beta P_{i\to f} = \mathbf{0}, \tag{9}$$

where $\mathbf{0}$ is a vector of zeros, implying that the gradient vectors $\nabla_\beta C$ and $\nabla_\beta P_{i\to f}$ are parallel at a suboptimal trap. The simple schematic topological sketches in Fig. 1 also need to be understood in terms of the demands expressed in Eq. (9), which are expanded further in Sect. 2.2 below.

2.2 Exploring local landscape topology at a trap

At a critical point, $dP_{i\to f}/ds = 0$, and exploring the local landscape while maintaining the $P_{i\to f}$ value to second order requires satisfying $d^2P_{i\to f}/ds^2 = 0$. This entails utilizing the second-order Hessian matrix, which is nominally comprised of the elements $\partial^2 P_{i\to f}/\partial\beta_m\partial\beta_n$, $m, n = 1, \ldots, M$. However, this form of the Hessian generally will not properly account for the inclusion of a constraint present on the β variables and thus may not reflect the constrained landscape topology. Here we derive an expression for the *constrained* Hessian that incorporates the function C and will be utilized to (1) identify local topology and (2) enable a landscape traversal in the neighborhood of a suboptimal critical point.

We introduce a new variable r for local critical point landscape exploration in order to distinguish it from the initial climbing trajectory monitored by s. To maintain $P_{i\to f}$ to second order, we wish to find an expression for $\partial\beta/\partial r$ that satisfies $d^2P_{i\to f}/dr^2 = 0$. Thus, differentiating Eq. (4) (i.e., understood with $s \to r$) and equating the result to zero yields

$$\nabla_\beta P_{i\to f}^\top \frac{\partial^2\beta}{\partial r^2} = -\sum_{m,n=1}^{M} \frac{\partial\beta_m}{\partial r}\frac{\partial^2 P_{i\to f}}{\partial\beta_m\partial\beta_n}\frac{\partial\beta_n}{\partial r}. \tag{10}$$

Similarly, we also demand that the constraint be maintained to second order such that differentiating Eq. (5) and equating the result to zero produces

$$\nabla_\beta C^\top \frac{\partial^2\beta}{\partial r^2} = -\sum_{m,n=1}^{M} \frac{\partial\beta_m}{\partial r}\frac{\partial^2 C}{\partial\beta_m\partial\beta_n}\frac{\partial\beta_n}{\partial r}. \tag{11}$$

We introduce the scalar function K,

$$K = \nabla_\beta P_{i\to f}^\top \nabla_\beta C \left(\nabla_\beta C^\top \nabla_\beta C\right)^{-1}. \tag{12}$$

and multiply Eq. (11) by K. Combining the latter result with Eqs. (8), (9), and (10) gives

$$\nabla_\beta P_{i\to f}^\top \frac{\partial^2\beta}{\partial r^2} = -\sum_{m,n=1}^{M} K\frac{\partial\beta_m}{\partial r}\frac{\partial^2 C}{\partial\beta_m\partial\beta_n}\frac{\partial\beta_n}{\partial r}. \tag{13}$$

By equating the right hand sides of Eqs. (10) and (13), we have

$$\sum_{m,n=1}^{M} \frac{\partial \beta_m}{\partial r} \frac{\partial^2 P_{i\to f}}{\partial \beta_m \partial \beta_n} \frac{\partial \beta_n}{\partial r} = \sum_{m,n=1}^{M} K \frac{\partial \beta_m}{\partial r} \frac{\partial^2 C}{\partial \beta_m \partial \beta_n} \frac{\partial \beta_n}{\partial r}, \tag{14}$$

which can be rewritten as

$$\sum_{m,n=1}^{M} \frac{\partial \beta_m}{\partial r} \left(\frac{\partial^2 P_{i\to f}}{\partial \beta_m \partial \beta_n} - K \frac{\partial^2 C}{\partial \beta_m \partial \beta_n} \right) \frac{\partial \beta_n}{\partial r} = 0. \tag{15}$$

This equation can be understood as specifying the local control changes (i.e., $\partial\beta/\partial r$) that preserve the constraint condition and the second term in parenthesis, $-K\nabla^2 C$, takes into account this condition. In this fashion the nominal Hessian $\nabla^2_\beta P_{i\to f}$ is amended to form the appropriate constrained Hessian $\mathcal{H}_C$ as

$$\mathcal{H}_C = \nabla^2_\beta P_{i\to f} - K\nabla^2_\beta C. \tag{16}$$

2.3 Moving on a suboptimal critical point level set

When the controls are not constrained, multiple solutions exist at the top of the transition probability landscape [15], which also implies an inherent degree of robustness to noise. In this circumstance, the family of multiple optimal solutions can be explored by requiring that control variations occur in the associated unconstrained Hessian (i.e., $\nabla^2_\beta P_{i\to f}$) null space, as this maintains the $P_{i\to f}$ value to second order. As indicated in Fig. 1b, a suboptimal critical point level set may also exist when operating with constrained controls. Thus, we now develop a methodology to traverse a suboptimal critical point level set, which utilizes the constrained Hessian $\mathcal{H}_C$ derived in Sect. 2.2. Specifically, we seek a form for $\partial\beta/\partial r$ that satisfies Eq. (15), written compactly as

$$\left(\frac{\partial \beta}{\partial r}\right)^\top \mathcal{H}_C \frac{\partial \beta}{\partial r} = 0. \tag{17}$$

While moving on the constrained level set we must still satisfy the constraint criterion in Eq. (5), which led to the relation in Eq. (7). In the present context we have

$$\frac{\partial \beta}{\partial r} = \mathcal{P}_C g \tag{18}$$

where $\mathcal{P}_C$ was given in Eq. (8) and the free function (vector) g will be specified below. Inserting Eq. (18) into Eq. (17) yields

$$g^\top \mathcal{P}_C \mathcal{H}_C \mathcal{P}_C g = 0, \tag{19}$$

leading to defining the *projected* Hessian as

$$\tilde{\mathcal{H}} = \mathcal{P}_C \mathcal{H}_C \mathcal{P}_C \tag{20}$$

so that Eq. (19) becomes

$$g^\top \tilde{\mathcal{H}} g = 0. \tag{21}$$

From Eqs. (18) and (21), moving on a suboptimal critical point level set will entail forcing changes in β to occur with g lying in the null space of the projected Hessian. Importantly, the projector $\mathcal{P}_C$, which in this work is formed based on the incorporation of a single constraint C, introduces one associated 'trivial' zero eigenvalue to the projected Hessian. In this circumstance, it is necessary for there to be at least two zero projected Hessian eigenvalues (i.e., to acceptable precision) in order to permit a traversal of a suboptimal critical point level set. Section 2.4 will present a method aiming to 'create' such nontrivial zero eigenvalues if none already exist by systematically morphing the *form* of the constraint. By denoting the projected Hessian zero eigenvectors by $\tilde{\nu}_j$, $j = 2, \ldots, J$, we can define g as

$$g = Qg' \tag{22}$$

$$= \left(\sum_{j=2}^{J} \tilde{\nu}_j \tilde{\nu}_j^\top \right) g' \tag{23}$$

where the counting starts with $j = 2$ as the first nontrivial null space eigenvector. Substituting Eq. (22) into Eq. (18) yields

$$\frac{\partial \beta}{\partial r} = \mathcal{P}_C Q g', \tag{24}$$

where g' is an arbitrary vector function whose choice will dictate the path taken on the level set. In this fashion Eq. (24) may be viewed as a differential equation for $\beta(r)$ whose solution along with the Schrödinger equation will permit a suboptimal critical point level set traversal.

2.4 Altering constraint-induced trap topology

In Sects. 2.1–2.3, the L constraint form parameters c of the function C were treated as fixed, implying that $C(\beta) = C_0$ maintained the same mathematical form while β changed. However, a topic of prime interest is the nature of how systematic relaxation of the constraint may lead to favorable topology changes. For example, transforming an isolated trap into a level set (c.f., changing Fig. 1a into Fig. 1b) can lead to identification of a family of homologous suboptimal controls, which implies an increased degree of robustness to noise and possibly opens up other ancillary properties for optimization. Alternatively, transforming a trap into a saddle (c.f., changing Fig. 1a into Fig. 1c) could permit further ascent of the $P_{i\to f}$ landscape. This section will introduce the mathematical procedure for relaxing the L constraint parameters while keeping $C =$

C_0 as well as the controls β fixed at their suboptimal trap values. Following the change in the constraint form parameters, movement in β can be considered to exploit the altered topology. Importantly, the consideration here of constraint form relaxation is of a limited nature through the parameters in c; the value of C_0 could also be considered for variation as well. In the most general context the constraints have a functional form for variation, but wide classes of constraint function form variations are permitted through c.

The parameter u is used to distinguish this new constraint parameter trajectory, where $c \to c(u)$. To enforce $C = C_0$, any change to c must satisfy

$$\frac{dC}{du} = \left(\frac{\partial C}{\partial c}\right)^{\top} \frac{\partial c}{\partial u} = 0. \tag{25}$$

We introduce the projector $\tilde{\mathcal{P}}$ into the space orthogonal to changes in $P_{i\to f}$,

$$\tilde{\mathcal{P}} = \mathbb{1} - \nabla_\beta P_{i\to f} (\nabla_\beta P_{i\to f}^{\top} \nabla_\beta P_{i\to f})^{-1} \nabla_\beta P_{i\to f}^{\top}. \tag{26}$$

Considering that $P_{i\to f}$ depends on M control variables β, we may define the $R = M - 1$ nonzero eigenvalues and eigenvectors of $\tilde{\mathcal{P}}$ by σ_k and w_k, respectively. Because we wish to maintain the trap condition in Eq. (9) of $\nabla_\beta P_{i\to f}$ and $\nabla_\beta C$ being parallel, any change to the constraint parameters c should satisfy

$$\tilde{\mathcal{P}} \nabla_\beta C = 0, \tag{27}$$

or equivalently

$$w_k^{\top} \nabla_\beta C = 0 \tag{28}$$

for $k = 1, \ldots, R$. Differentiating Eq. (28) with respect to u and noting that $P_{i\to f}$ does not explicitly depend on c yields

$$w_k^{\top} \Lambda \frac{\partial c}{\partial u} = 0 \tag{29}$$

where Λ is an $M \times L$ matrix with elements

$$\Lambda_{ml} = \frac{\partial^2 C}{\partial \beta_m \partial c_l}. \tag{30}$$

Equations (25) and (29) are both of the form

$$p^{\top} \frac{\partial c}{\partial u} = 0 \tag{31}$$

where p is a length-L vector. An $L \times M$ matrix Ω may be formed from the M equations arising from (25) and (29), where

$$\Omega = \begin{pmatrix} | & & | \\ p_1 & \cdots & p_M \\ | & & | \end{pmatrix}. \tag{32}$$

An $L \times L$ projector matrix $\mathcal{P}_\Omega$ is formed from Ω as

$$\mathcal{P}_\Omega = \mathbb{1} - \Omega(\Omega^\top \Omega)^{-1}\Omega^\top, \tag{33}$$

where the matrix $\Omega^\top\Omega$ is assumed to be invertible. We may then write the differential change in c as satisfying

$$\frac{\partial c}{\partial u} = \mathcal{P}_\Omega h \tag{34}$$

with a function vector h that can be freely chosen to satisfy an ancillary objective. In particular, below we will show that h can be chosen with the goals of seeking to (i) transform a trap into a level set (i.e., Fig. 1a into Fig. 1b) or (ii) change a trap into a saddle (i.e., Fig. 1a into Fig. 1c).

2.4.1 Changing a trap into a level set

To vary the constraint parameters c to enable the landscape topology transformation represented by L_1 in Fig. 1, we can express the goal through manipulation of the eigenspectrum of the projected Hessian $\tilde{\mathcal{H}}$ following from Sect. 2.3. We seek (nontrivial) zero projected Hessian eigenvalues $\tilde{\lambda}_j$ and employ the cost function

$$\mathcal{L}_1 = \mathrm{Tr}(\tilde{H}^2) = \sum_j (\tilde{\lambda}_j)^2. \tag{35}$$

The goal is to minimize $\mathcal{L}_1$ over c hoping that at least one nontrivial new zero eigenvalue appears to acceptable precision. Differentiating $\mathcal{L}_1$ with respect to u yields

$$\frac{d\mathcal{L}_1}{du} = \left(\frac{\partial \mathcal{L}_1}{\partial c}\right)^\top \frac{\partial c}{\partial u}, \tag{36}$$

where substitution of Eq. (34) results in

$$\frac{d\mathcal{L}_1}{du} = \left(\frac{\partial \mathcal{L}_1}{\partial c}\right)^\top \mathcal{P}_\Omega h. \tag{37}$$

Minimization of $\mathcal{L}_1$ can be accomplished by choosing $h = -\partial\mathcal{L}_1/\partial c$. The sequential operation of minimization of $\mathcal{L}_1$ and a level set traversal likely will call for iterative, incremental steps, likened to the desired level set being a carpet rolled forward where the next step depends on the previous one.

2.4.2 Changing a trap into a saddle

To vary the constraint parameters to perform the topological transformation L_2 in Fig. 1, the cost function

$$\mathcal{L}_2 = \mathrm{Tr}(\mathcal{H}_C) = \sum_m \lambda_m \tag{38}$$

is utilized. Here, the aim is to maximize $\mathcal{L}_2$, which depends on the constrained Hessian $\mathcal{H}_C$ derived in Sect. 2.2, whose eigenvalues are denoted by λ_m. Recall that the level set traversal algorithm from Sect. 2.3 required projecting changes in the controls to occur in the null space of the *projected* Hessian $\tilde{\mathcal{H}}$. However, in the case of creating a saddle we are only concerned with the eigenspectrum of the *constrained* Hessian, as subsequent landscape ascent can be accomplished by either moving in the direction of newly formed positive $\mathcal{H}_C$ eigenvalues, or possibly by again employing the first-order ascent procedure from Sect. 2.1. Following Eq. (37), we set $h = \partial\mathcal{L}_2/\partial c$ to maximize $\mathcal{L}_2$.

There is no guarantee that either of the goals in Sects. 2.4.1 or 2.4.2 may be achieved with any particular chosen form of constraint relaxation. Importantly, exploration of this issue is enabled by the tools above, especially consideration of whether minimal levels of relaxation may have significant impact on the apparent constrained landscape topology.

3 Numerical illustrations

The simulations presented in this work aim to illustrate employment of the generic mathematical tools developed in Sect. 2 using simple model systems and associated model dynamic controls. For the purpose of illustration, the control variables β are chosen as the amplitudes of a field, where

$$\varepsilon(t) = \exp\left(-\frac{8\pi}{T^2}\left(t - \frac{T}{2}\right)\right)\sum_{m=1}^{M}\beta_m \sin(\omega_m t + \phi_m), \tag{39}$$

though other dynamic controls such as phase parameters could also be used. The choice of field form in Eq. (39) is itself a constraint, although with sufficient terms M and reasonable choices for the frequencies ω_m, the free manipulation of the parameters β_m and ϕ_m can generally satisfy the resource assumption (3) discussed in Sect. 1. Here, we will impose significant constraints to illustrate behavior in the domain of limited dynamic resources. All units in the following simulations are arbitrary. The form of the imposed constraint function C will be provided in each case below.

3.1 Ascending the $P_{i\to f}$ landscape with constrained amplitude controls

We begin by implementing the first-order landscape ascent algorithm described in Sect. 2.1. The system has dimension $N = 4$. The Hamiltonian in Eq. (3) has H_0 diagonal elements

$$H_0 = [8.6532, 10.2908, 12.1528, 13.8258]$$

and μ contains

$$\mu = [\mu(1,1) = 0.1353, \mu(2,2) = 0.0033, \mu(3,3) = 0.3933, \mu(4,4) = 0.2736, \mu(1,2) = 0.0226, \mu(1,3) = 0.2242, \mu(1,4) = 0.2742, \mu(2,3) = 0.2254, \mu(2,4) = 0.1213, \mu(3,4) = 0.2031].$$

$P_{i\to f}$ was chosen as $P_{1\to 4}$ with the understanding that this is potentially a demanding objective to optimize under constrained control resources. This example will be used in Sect. 3.2.1 as a starting point to implement the transformation L_1 in Fig. 1. A second landscape climb with a different system will be performed in Sect. 3.2.2 as a basis for illustrating the transformation L_2 in Fig. 1.

An initial control field $\varepsilon(t)$ of the form in Eq. (39) was generated with $M = 10$ frequency components resonant with the energy transitions arising from H_0 and 10 randomly chosen amplitudes and phases from the domains [0, 1] and $[0, 2\pi]$, respectively. The final time was $T = 10$. After the phases were randomly chosen, they were no longer varied, thereby just limiting the control to the coefficients β_m.

A subset $\tilde{\beta}$ of β was subjected to the constraint

$$C(s) = \frac{1}{M'} \sum_{m'=1}^{M'} (\tilde{\beta}_{m'}(s))^2 = C_0, \tag{40}$$

where $M' = 8$ and $\tilde{\beta} = [\beta_1, \ldots, \beta_6, \beta_8, \beta_{10}]$. This implies that the two amplitudes β_7 and β_9 may freely vary (i.e., without being constrained by C). The form for C in Eq. (40) is used for illustrative purposes and many other forms may be considered. Importantly, $M = 10$ (i.e., the total number of constrained and unconstrained controls) is larger than $2N - 2 = 6$, which has been found to be the number of independent properly chosen control variables generally required for complete $P_{i\to f}$ control [14]. Here we explore the impact of the imposed 'function' constraint in Eq. (40), rather than working with an insufficient number of controls, which has been considered in previous work [8].

Given an initial set of amplitudes $\beta \in [0, 1]$, the resultant value of $C_0 = 0.2925$ was demanded to remain fixed during the optimization of $P_{1\to 4}$. As the amplitudes morph during the $P_{1\to 4}$ ascent, C was maintained on the order of 10^{-8}, and $P_{1\to 4}$ monotonically increased from 0.1556 to 0.6119 as shown in Fig. 2a. At $P_{1\to 4} = 0.6119$, no variation to the control variables could result in further increase in $P_{1\to 4}$ with the imposed constraint from Eq. (40). The values for all $M = 10$ parameters β_m at $P_{1\to 4} = 0.1556$ and 0.6119 are shown in Fig. 2b. While the initial amplitudes were chosen from the domain [0, 1] (upright triangles in Fig. 2b), no effort was made to constrain the amplitudes to reside within this region during the landscape trajectory. The control that changes the most during the optimization is β_7, which is not an element of $\tilde{\beta}$. The control β_9, also not in $\tilde{\beta}$, changed much less by comparison. The control amplitudes vary in a coordinated, albeit partially constrained manner to increase $P_{1\to 4}$ until $dP_{1\to 4}/ds = 0$.

To determine the local landscape topology at $P_{1\to 4} = 0.6119$, the constrained Hessian $\mathcal{H}_C$ (c.f., Eq. 16) was computed, and its eigenvalues are shown in Fig. 3. All

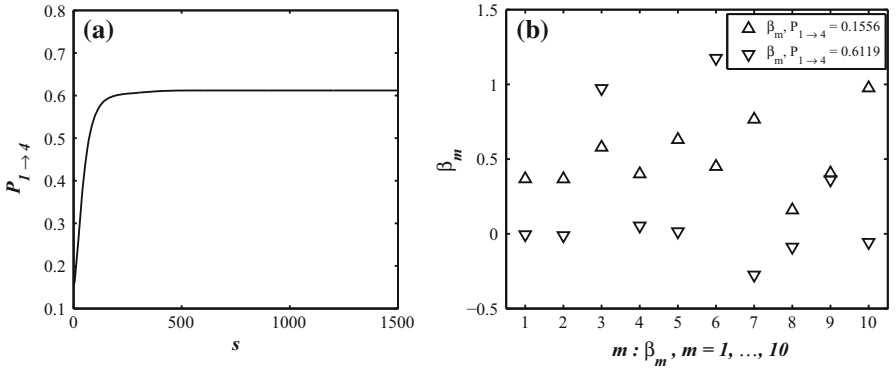

Fig. 2 **a** Optimization of $P_{1\to4}$ where the field had ten amplitudes as the control variables (c.f., Eq. 39). 8 of these amplitudes ($\tilde{\beta}$; see Sect. 3.1) are subject to the constraint C in Eq. (40); β_7 and β_9 are permitted to freely vary. $P_{1\to4}$ increases from 0.1556 to 0.6119, where a constraint-induced critical point is encountered. The amplitudes corresponding to the initial landscape point at $P_{1\to4} = 0.1556$ are shown as *upright triangles* in (**b**). The amplitudes corresponding to $P_{1\to4} = 0.6119$ are shown as *inverted triangles* in (**b**). The initial amplitudes are randomly chosen from the domain [0, 1], and no attempt was made to keep the amplitudes within this range during optimization. The amplitudes changed in a complex and coordinated manner to achieve the best accessible $P_{1\to4}$ yield

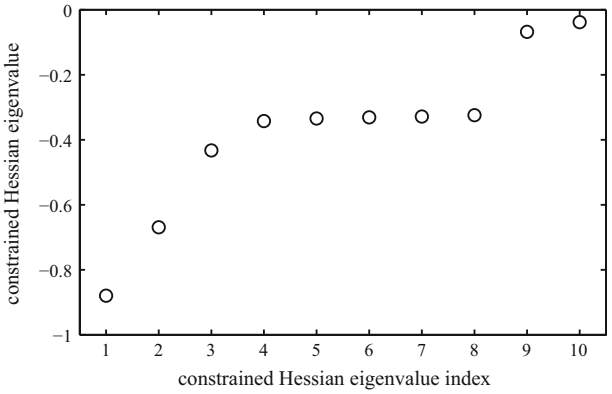

Fig. 3 Eigenvalues of the constrained Hessian (c.f., Eq. 16) at the trap encountered at $P_{1\to4} = 0.6119$ in Fig. 2a. All eigenvalues are negative and range from −0.8798 to −0.0383, implying that the trap exists as an isolated point on the control landscape

the eigenvalues are negative and range from −0.8798 to −0.0383. This circumstance implies that the encountered critical point is an isolated suboptimal trap with a topology like that displayed in Fig. 1a, such that any change in the defined controls induced by noise or other variations would result in a decrease in $P_{1\to4}$. In Sect. 3.2.1, we will transform this isolated trap into a level set represented by the change in going from Fig. 1a to Fig. 1b.

3.2 Altering apparent trap topology

The transformations of landscape topology indicated in Fig. 1 will be illustrated below. Section 3.2.1 will utilize the case from Sect. 3.1 and Fig. 2 to create a trap → level

set transformation along with a traversal of the resultant level set. Section 3.2.2 will utilize a different system to illustrate the trap → saddle transformation along with subsequent further ascent of the landscape.

3.2.1 Turning an isolated point into a level set

In order to employ the methodology presented in Sect. 2.4 in an attempt to change the topology of the encountered trap in Sect. 3.1, a set of L constraint parameters c are introduced in C. In this fashion, we consider the simple case of $C \rightarrow C'$, where

$$C' = \frac{1}{M'} \sum_{m'=1}^{M'} (\tilde{\beta}_{m'} - c_{m'})^2 + c_{M'+1} \equiv C_0, \tag{41}$$

where $c_{M'+1}$ is included to compensate as needed for the variations of $c_{m'}, m' = 1, \ldots, M'$ and maintain $C' = C_0$. The change in form provided by Eq. (41) may be viewed as a bias for the subsequent changes in β once the topology has been changed. More radical changes in the form for $C(\beta)$ could be considered as well, while the subtle shift provided by Eq. (41) will be shown to already have a significant impact on the local topology of the landscape. Consistent with the original constraint in Eq. (40), the length $L = M' + 1 = 9$ vector of constraint parameters c may be viewed as zero during the initial landscape ascent in Fig. 2. The goal now is to morph c, while β are fixed, in order to change the encountered isolated trap at $P_{1\rightarrow 4} = 0.6119$ into a level set using the formulation laid out in Sect. 2.4. After morphing c, the control variables β will be subject to further constrained variation within Eq. (41) in order to move on the newly opened up level set.

Figure 4a shows the initial and final values for the nine elements of c as they are morphed in an effort to create nontrivial projected Hessian eigenvalues through minimization of $\mathcal{L}_1$ in Eq. (35). Since $P_{1\rightarrow 4}$ is independent of c, it remains unchanged during the constraint morphing procedure. The constraint $C' = C_0 = 0.2925$ was maintained on the order of 10^{-8} during the morphing of c. The search procedure was terminated when a single nontrivial projected Hessian eigenvalue on the order of 10^{-5} was identified; additional 'null' eigenvalues might be discovered upon further searching. Correspondingly, $\mathcal{L}_1$ monotonically decreased from 1.5101 to 0.5264. In Fig. 4a, the constraint parameter that changes the most is c_9, which compensates for the changes in c_1 through c_8 while the constraint function $C' = C_0$ is maintained. Figure 4b displays the projected Hessian eigenvalues before and after the constraint parameter morphing procedure, where $\tilde{\lambda}_9$ evolves to 10^{-5} (noting that $\tilde{\lambda}_{10}$ represents the trivially zero eigenvalue of $\tilde{\mathcal{H}}$).

The breadth of a landscape level set may depend on a number of factors, including the permitted change in the observable value defined as acceptable and appropriate tolerances in control variation. In this simulation, a level set was defined by allowing $P_{1\rightarrow 4}$ to vary no more than 10^{-4}. Using the initially trapped controls β^{trap},

$$\begin{aligned} \beta^{trap} = [&-0.0053, -0.0114, 0.9725, 0.0530, 0.0147, 1.1747, \\ &-0.2757, -0.0888, 0.3615, -0.0568] \end{aligned} \tag{42}$$

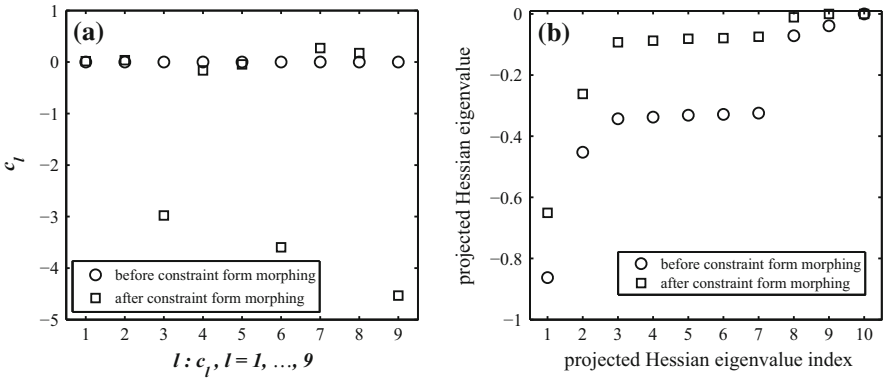

Fig. 4 Using the constraint parameter morphing procedure laid out in Sect. 2.4, a set of $M' + 1 = 9$ constraint parameters c were varied in an effort to change the topology of the $P_{1\to 4}$ trap from an isolated point into a level set. The evolution of constraint parameters $c_l, l = 1, \ldots, 9$ is shown in (**a**). All c_l are initially zero and evolve according to the minimization of $\mathcal{L}_1$ in Eq. (35). The largest change occurs for c_9, per Eq. (41) evidently to compensate for the changes in c_1 through c_8. The projected Hessian (c.f., Eq. 20) eigenvalues before and after the constraint parameter morphing technique is employed are shown in (**b**). One (nontrivial) eigenvalue on the order of 10^{-5} was identified (index 9) and judged sufficiently 'zero' to use for subsequent level set traversal. $\mathcal{L}_1$ decreased from 1.5101 to 0.5264

and the morphed values for c (i.e., the squares in Fig. 4a), the controls were varied according to the second-order procedure described in Sect. 2.3. The free function g' (c.f., Eq. 24) was a randomly generated vector held fixed while performing the level set trajectory. The trajectory was halted when $P_{1\to 4}$ changed by more than 10^{-4}, resulting in the final control parameters

$$\begin{aligned}\beta^{ls} = [&-0.0159, -0.0207, 0.9677, 0.2159, 0.1678, 1.1582,\\ &-0.2676, -0.1141, 0.6307, -0.1252].\end{aligned} \tag{43}$$

The overall changes, $\beta^{trap} \to \beta^{ls}$, are quite significant. The projected Hessian eigenvalues were computed at this new value of β^{ls} and it was observed that the smallest nontrivial eigenvalue had increased to 10^{-3}; practice indicates that a null eigenvalue needs to be $\sim 10^{-5}$ in order to perform a level set trajectory and keep $P_{i\to f}$ fixed to acceptable accuracy. The constraint parameter morphing procedure could be initiated again starting at β^{ls} to attempt to find at least one new nontrivial zero projected Hessian eigenvalue and then take another step. Such an iterative process could be employed as a means to explore the boundary of a trap level set to specified precision. The use of a different free function g' also results in distinct level set traversals and different values for the controls.

3.2.2 Turning an isolated point into a saddle

The topological transformation performed in Sect. 3.2.1 turned an isolated trap into a level set, which was accomplished through minimization of $\mathcal{L}_1$ (c.f., Eq. 35) via controlled variations of the constraint parameters c. Now we demonstrate the alternative

capability of turning an isolated trap into a saddle. Thus, we seek a c that produces at least one positive constrained Hessian eigenvalue.

A new $N = 4$-dimensional system is considered, where the diagonal elements of H_0 and the matrix μ are

$$H_0 = [0.0534, 0.4873, 6.6637, 15.8803]$$

$$\begin{aligned}\mu = [&\mu(1,1) = 0.3300, \mu(2,2) = 0.0522, \mu(3,3) = 0.1688, \mu(4,4) = 0.3073,\\ &\mu(1,2) = 0.2093, \mu(1,3) = 0.3685, \mu(1,4) = 0.1752, \mu(2,3) = 0.1498,\\ &\mu(2,4) = 0.2885, \mu(3,4) = 0.2420]\end{aligned}$$

and amplitude controls are again employed. A resonant initial field of the form in Eq. (39) was generated, where $M = 15$ amplitudes and phases were initially randomly chosen from the domains $[0, 1]$ and $[0, 2\pi]$, respectively. In contrast to the simulations above where only a subset of the field amplitudes β were incorporated in a function constraint, in this example we considered all $M = 15$ amplitudes to be constrained following C in Eq. (40) (i.e., where $M' = M = 15$). The initial random choice of β produced $C_0 = 0.3714$, which was demanded to remain fixed during a constrained optimization of $P_{1\to4}$. An isolated trap was encountered at $P_{1\to4} = 0.2212$, where all constrained Hessian eigenvalues were negative (results not shown).

A set of $L = M + 1 = 16$ constraint parameters was incorporated into Eq. (41). Figure 5a shows the initial and final values for c as they vary to produce at least one positive constrained Hessian eigenvalue through maximization of $\mathcal{L}_2$ in Eq. (38). The constraint $C' = 0.3714$ was maintained on the order of 10^{-7} during the evolution of c. The constraint morphing procedure was terminated when a posi-

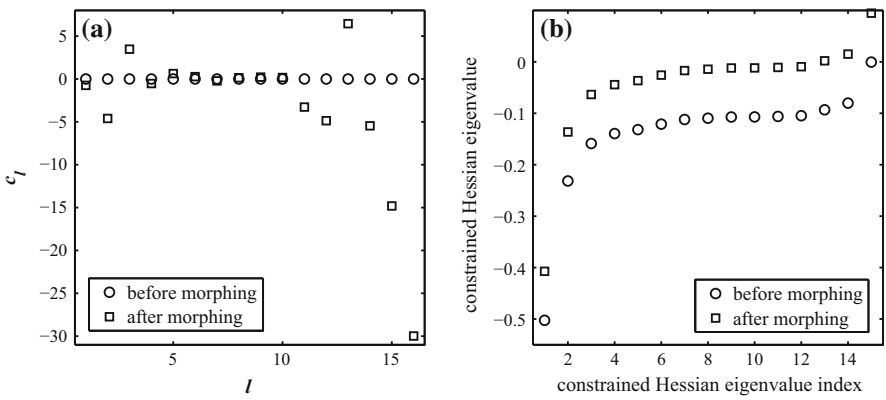

Fig. 5 Using the procedure laid out in Sect. 2.4, a set of 16 constraint parameters c (all initially zero) are allowed to morph in an effort to change the topology of the $P_{1\to4} = 0.2212$ trap from an isolated point into a saddle. The function $\mathcal{L}_2$ (c.f., Eq. 38) is maximized during the variation of c. In (**a**), the constraint parameters evolve from circles to squares. In (**b**), the evolution of the constrained Hessian eigenvalues is monitored; the *squares* represent the eigenvalues identified at the final stage of the constraint morphing procedure. Three positive eigenvalues are identified, which correspond to directions in which the controls (e.g., amplitudes) may change to possibly further ascend the $P_{1\to4}$ landscape

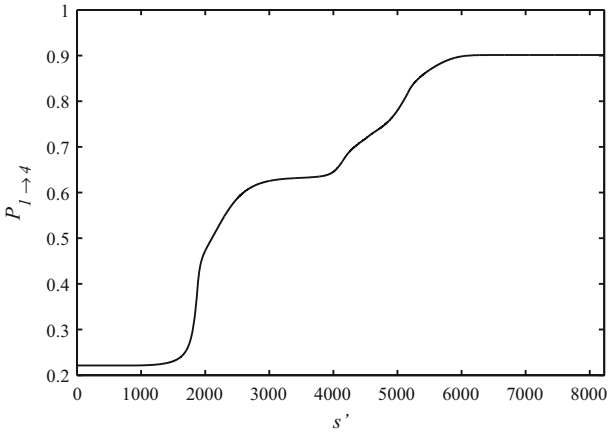

Fig. 6 Increase in $P_{1\to4}$ over variation in control amplitudes after morphing of the constraint parameters c to identify a saddle in Fig. 5. The first-order landscape ascent algorithm from Sect. 2.1 was employed. In this case, the imposed constraint assumes the form C' (c.f., Eq. 41), where the values for c are identified as *squares* in Fig. 5a. A gradient algorithm was able to morph the amplitudes resulting in a climb from the initial trap at $P_{1\to f} = 0.2212$ to eventually reach $P_{1\to4} = 0.9011$, where another trap is encountered. Another saddle region appears to be approached near $s' \sim 3{,}000{-}4{,}000$, but the controls continue to change and move around the new saddle so as to further ascend the landscape

tive eigenvalue on the order of $\sim 10^{-1}$ was identified. In this example, $\mathcal{L}_2$ increased from -2.1062 to -0.6778. Figure 5b displays the corresponding initial constrained Hessian eigenvalues (i.e., when $c_l = 0, l = 1, \ldots, 16$). Three positive eigenvalues are identified at the end of the constraint morphing procedure, suggesting that with coordinated variations in the amplitude controls, as dictated by eigenvectors associated with the positive eigenvalues, further ascent of the $P_{1\to4}$ landscape should be possible. While it is feasible to directly 'follow' these directions of positive curvature (i.e., using second-order constrained Hessian information), we now test whether the landscape can be climbed by reverting to the first-order ascent algorithm from Sect. 2.1.

The vector c was fixed at its morphed values (i.e., those represented as squares in Fig. 5a), and the first-order constrained D-MORPH landscape ascent procedure was utilized with the imposed constraint $C' = 0.3714$. The amplitudes started from their trapped values, and Fig. 6 shows the increase in $P_{1\to4}$ where the index s' is used to distinguish this climb from the ascent to the trap at $P_{1\to4} = 0.2212$. Initially, the new climb is slow, but near $s' \sim 1{,}500$ the algorithm is able to 'locate' the direction of positive landscape curvature as indicated by the positive constrained Hessian eigenvalues. A distinct feature seen in Fig. 6 is that another saddle seems to be encountered on the climb in the window $s' \sim 3{,}500{-}4{,}000$, where the climb slows. The controls eventually escape the additional saddle region and climb to a higher $P_{1\to4}$ value. However, a new trap is encountered at $P_{1\to4} = 0.9011$, as confirmed from the eigenvalues of $\mathcal{H}_C$ being all negative (not shown). The fields corresponding to the control amplitudes at $P_{1\to4} = 0.2212$ and 0.9011 are shown in Fig. 7 as solid and dash-dot curves, respectively. While complete control was not attained, a dra-

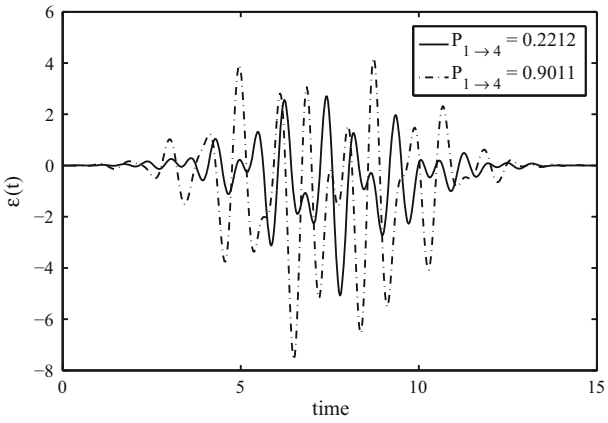

Fig. 7 Control fields corresponding to the amplitudes at $P_{1\to 4} = 0.2212$ (*solid curve*) and 0.9011 (*dash-dot curve*) from Fig. 6. While complete control is not achieved, a substantial increase in $P_{1\to 4}$ was accomplished through variation of constrained controls after morphing of the constraint parameters in the transformation of a trap into a saddle

matic increase in $P_{1\to 4}$ was achieved, indicating that systematic relaxation of control resources can permit landscape topology variation that potentially allows for increased control.

4 Conclusions

In any quantum control experiment, constraints on resources are unavoidable. In an experimental setting, one must consider the tradeoff between control fidelity and the costs of constraint relaxation. Understanding the role of constraints in achieving optimal control and their impact on apparent control landscape topology remains an important research goal, and the present work is a step towards that aim. This paper worked with natural physical variables arising in $\varepsilon(t)$, in contrast to prior constrained quantum control studies that utilized more abstract kinematic variables [10,11]. An algorithm was presented to ascend the transition probability landscape under arbitrary constrained controls until a critical point is reached. The local landscape topology about the critical point can be explored through an examination of the constrained Hessian. A mathematical methodology was presented that enables seeking topological transformations at suboptimal traps through systematic variation of a set of constraint parameters, introduced to alter the form of the constraint. The tools introduced here are general thereby permitting consideration of a variety of control-constraint form pairings. Numerical simulations were presented in Sect. 3 for simple cases to illustrate the tools laid out in Sect. 2. A set of dynamic control variables first encountered a suboptimal trap during a constrained landscape ascent. One example showed the capability of the constraint parameter morphing procedure to transform an isolated trap into a level set, followed by traversal on the newly created level set over a sequence of distinct, homologous controls. A second example demonstrated a transformation of an isolated trap into a saddle, permitting subsequent climbing to a much higher yield.

Iteration of these procedures will generally be required to make larger excursions over the landscape.

The complex interplay between controls and constraints make it virtually impossible to know a priori how to relax the constraints, especially in a minimal fashion, to achieve enhanced control performance. The procedures developed here enable judicious systematic variations of control resources to explore their effects on apparent constrained landscape topology. The controls may also be expanded to include the Hamiltonian structure (i.e., H_0 and/or μ) as resources when system engineering or manipulation is possible [16–18]. Thus, future studies may explore a variety of possible control variables and constraints to investigate the rich nature of constrained control landscape topology.

Acknowledgments A.D. acknowledges support from the Program in Plasma Science and Technology at Princeton University and the NSF (CHE-1058644), ARO (W911NF-13-1-0237), and ARO-MURI (W911NF-11-1-2068). H.R. acknowledges partial support from DOE (DE-FG02-02ER15344).

References

1. C. Brif, R. Chakrabarti, H. Rabitz, Control of quantum phenomena: past, present and future. New J. Phys. **12**, 075008 (2010)
2. H. Rabitz, M. Hsieh, C. Rosenthal, Quantum optimally controlled transition landscapes. Science **303**, 1998 (2004)
3. V. Ramakrishna, M. Salapaka, M. Dahleh, H. Rabitz, A. Pierce, Controllability of molecular systems. Phys. Rev. A **51**, 960 (1995)
4. S. Schirmer, H. Fu, A. Solomon, Complete controllability of quantum systems. Phys. Rev. A **63**, 063410 (2001)
5. J. Werschnik, E. Gross, Tailoring laser pulses with spectral and fluence constraints using optimal control theory. J. Opt. B **7**, S300 (2005)
6. M. Lapert, R. Tehini, G. Turinici, D. Sugny, Monotonically convergent optimal control theory of quantum systems with spectral constraints on the control field. Phys. Rev. A **79**, 063411 (2009)
7. P. von den Hoff, S. Thallmair, M. Kowalewski, R. Siemering, R. de Vivie-Riedle, Optimal control theory-closing the gap between theory and experiment. Phys. Chem. Chem. Phys. **14**, 14460 (2012)
8. K. Moore, H. Rabitz, Exploring constrained quantum control landscapes. J. Chem. Phys. **137**, 134113 (2012)
9. C.-C. Shu, N. Henriksen, Phase-only shaped laser pulses in optimal control theory: application to indirect photofragmentation dynamics in the weak-field limit. J. Chem. Phys. **136**, 044303 (2012)
10. A. Donovan, V. Beltrani, H. Rabitz, Exploring the impact of constraints in quantum optimal control through a kinematic formulation. Chem. Phys. **425**, 46 (2013)
11. A. Donovan, V. Beltrani, H. Rabitz, Local topology at limited resource induced suboptimal traps on the quantum control landscape. J. Math. Chem. **52**, 407 (2014)
12. A. Donovan, H. Rabitz, Investigating constrained quantum control through a kinematic-to-dynamic variable transformation. Phys. Rev. A **90**, 013408 (2014)
13. A. Rothman, T.-S. Ho, H. Rabitz, Exploring the level sets of quantum control landscapes. Phys. Rev. A **73**, 053401 (2006)
14. H. Rabitz, T.-S. Ho, M. Hsieh, R. Kosut, M. Demiralp, Topology of optimally controlled quantum mechanical transition probability landscapes. Phys. Rev. A **74**, 012721 (2006)
15. V. Beltrani, J. Dominy, T.-S. Ho, H. Rabitz, Exploring the top and bottom of the quantum control landscape. J. Chem. Phys. **134**, 194106 (2011)
16. A. Persidis, High-throughput screening. Nat. Biotechnol. **5**, 488 (1998)
17. A. Donovan, V. Beltrani, H. Rabitz, Quantum control by means of hamiltonian structure manipulation. Phys. Chem. Chem. Phys. **13**, 7348 (2011)
18. C. Wedge, G. Timco, E. Spielberg, R. George, F. Tuna, S. Rigby, E. McInnes, R. Winpenny, S. Blundell, A. Ardavan, Chemical engineering of molecular qubits. Phys. Rev. Lett. **108**, 107204 (2012)